



# New N-Heterocyclic Compounds Based on 8-Hydroxyquinoline as Efficient Corrosion Inhibition for Mild Steel in HCl Solution: Experimental and Theoretical Assessments

M. Rbaa<sup>1</sup> · Ashraf S. Abousalem<sup>2,3</sup> · M. Galai<sup>4</sup> · H. Lgaz<sup>5</sup> · B. Lakhrissi<sup>1</sup> · I. Warad<sup>6</sup> · A. Zarrouk<sup>7</sup>

Received: 8 October 2019 / Accepted: 25 May 2020 / Published online: 3 June 2020  
© King Fahd University of Petroleum & Minerals 2020

## Abstract

Both new benzimidazole derivatives based on 8-hydroxyquinoline, namely 4-(1-((4-hydroxynaphthalen-1-yl)methyl)-5-methyl-1*H*-benzo[d]imidazol-2-yl)benzoic acid (QN1) and 4-(1-((4-hydroxynaphthalen-1-yl)methyl)-1*H*-benzo[d]imidazol-2-yl)benzoic acid (QN2), were synthesized and characterized, and their corrosion inhibition behavior as well as the mechanism of inhibition was investigated by different techniques. Structural characterization includes NMR, IR and elemental analysis. The anticorrosive activity of these compounds was evaluated by the potentiodynamic polarization and impedance spectroscopy. Experimental data show that the QN1 and QN2 are effective against corrosion of steel in 1.0 M HCl and that the inhibitory efficiency reached at an optimum value of 97.7% for the QN1 compound at 1 mm. Polarization Tafel curves show that QN1<sub>1</sub> and QN2 act as a mixed type of inhibitors. After evaluating the anticorrosive activity of these two compounds, we used the surface techniques, namely SEM coupled with EDS and the gravimetric solutions were analyzed by UV–visible spectrometry. Quantum mechanical investigations density functional theory calculations and the Monte Carlo simulation on corrosion behavior of QN1 and QN2 compounds were also conducted, and satisfying correlation was noticed between the results of corrosion measurement methods and quantum mechanical evaluations.

**Keywords** Benzimidazole · 8-Hydroxyquinoline · Corrosion Inhibition · Mild steel · Monte Carlo simulation · DFT · UV–visible spectrometry

## 1 Introduction

The industries are based on a large amount of their manufacture on metals, especially mild steel due to its remarkable importance in nearly every sphere of life and

industrial applications like mechanical equipment, ships, marine structures, process industries, power plants and building construction [1–3]. The mild steel until today is deteriorated by the corrosion in the aggressive environment, notably the acids [4]. From an economic, there is an urgent need to innovative new solution to control mild steel corrosion. During the past decade, a number of inhibitors have been reported. Most of the effective corrosion

**Electronic supplementary material** The online version of this article (<https://doi.org/10.1007/s13369-020-04667-4>) contains supplementary material, which is available to authorized users.

✉ M. Rbaa  
mohamed.rbaa10@gmail.com

✉ A. Zarrouk  
azarrouk@gmail.com

<sup>1</sup> Laboratory of Agro-Resources, Polymers and Process Engineering, Faculty of Sciences, Ibn Tofail University, PO Box 133, 14000 Kenitra, Morocco

<sup>2</sup> Quality Control Laboratory, JOTUN, New Cairo, Egypt

<sup>3</sup> Chemistry Department, Faculty of Science, Mansoura University, Mansoura, Egypt

<sup>4</sup> Laboratory of Materials Engineering and Environment: Modeling and Application, Faculty of Science, Ibn Tofail University, BP 133-14000, Kenitra, Morocco

<sup>5</sup> Department of Crop Science, College of Sanghur Life Science, Konkuk University, Seoul 05029, South Korea

<sup>6</sup> Department of Chemistry and Earth Sciences, Qatar University, PO Box 2713, Doha, Qatar

<sup>7</sup> Laboratory of Materials, Nanotechnology and Environment, Faculty of Sciences, Mohammed V University, Av. Ibn Battuta, P.O. Box 1014, Rabat, Morocco



inhibitors are organic compounds, which contain electronegative atoms (such as nitrogen, phosphorus, sulfur and oxygen atoms), the unsaturated bonds (such as double bonds or triple bonds) and the plane conjugated systems including all kinds of aromatic cycles in their molecular structures [5–10]. In addition, the geometric flatness of a molecule is a very important factor that will help this molecule to adsorb well on the metal surface [11].

The *8-hydroxyquinoline* derivatives are proved good corrosion inhibitors for steels, especially in the hydrochloric acid medium [12–16]. In our previous works, we have successfully prepared some *8-hydroxyquinoline* derivatives and applied them in the inhibition of steel corrosion and as a powerful antibacterial agent [17]. On the other hand, over the past years, the *benzimidazoles* derivatives have gained great attention due to their unique properties. This class of organic compounds, in general, contains many advantages, which has increased their application as corrosion inhibitors [18]. Recently, several works have been published on the inhibition of corrosion of certain derivatives of 8-hydroxyquinoline used as corrosion inhibitors in hydrochloric acid medium. It is noted that all substituted quinoline compounds act as good corrosion inhibitors and their inhibition increase with their concentrations [19, 20]. The use of the quinoline derivatives as corrosion inhibitors have been widely reported by several authors [21, 22]. As an example, Table 1 reports the percentage inhibition efficiency for some selected quinoline derivatives used as corrosion inhibitors in 1.0 M HCl medium. The values of inhibition efficiency, given in this table, were obtained using EIS measurement after 1/2 h of immersion in 1.0 M HCl solution containing  $10^{-3}$  M of quinoline derivative at 298 K. By comparing these data, we can show that our quinoline derivative (QN1) is the best effective inhibitor in 1.0 M HCl. Moreover, we get a high value of efficiency even at a lower concentration of this quinoline derivative (93.5% at  $10^{-6}$  M of QN1).

The novelty of this work were the synthesization of two new polyfunctional heterocyclic products based on 8-hydroxyquinoline and the characterization of these compounds using IR, NMR spectroscopy and elemental analysis methods. However, we tested the two new synthesized compounds as a corrosion inhibitor for M-steel in 1.0 M HCl. The corrosion study was carried out by the electrochemical (PDP and EIS study) and theoretical techniques (DFT calculations and Monte Carlo simulation). However, we tested the two new synthesized compounds as a corrosion inhibitor for M-steel in 1.0 M HCl. The corrosion study was carried out by the electrochemical (PDP and EIS study) and theoretical techniques (DFT calculations and Monte Carlo simulation). The metal surface was characterized by SEM coupled with EDS, and the gravimetric solutions were analyzed by UV–visible spectrometry.

## 2 Materials and Methods

### 2.1 Synthesis of N-Heterocyclic Compounds *Benzimidazole* Based on *8-Hydroxyquinoline* QN1 and QN2

The synthesis of *benzimidazole* compounds based on *8-hydroxyquinoline* was carried out in three steps:

The first step is the preparation of the *benzimidazole* derivatives (**1** and **2**) by the reaction of ortho-phenylenediamine with 4-formylbenzoic acid in dimethylformamide (DMF) at reflux, in the presence of sodium dithionite ( $\text{Na}_2\text{S}_2\text{O}_4$ ) for activation of the aldehyde function. The second step is the preparation of *5-chloromethyl-8-hydroxyquinoline* from *8-hydroxyquinoline* (**3**) by acid bubbling at room temperature for 24 h. The last step consists in condensing the *benzimidazole* derivatives (**1** and **2**) with *5-chloromethyl-8-hydroxyquinoline hydrochloride* (**3**) in acetonitrile ( $\text{CH}_3\text{CN}$ ) in the presence of potassium carbonate ( $\text{K}_2\text{CO}_3$ ) at refluxing for 24 h.

### 2.2 Procedure

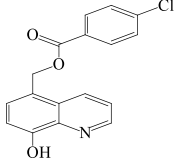
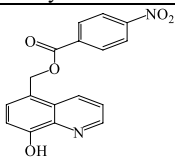
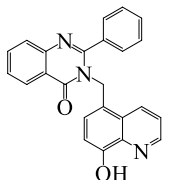
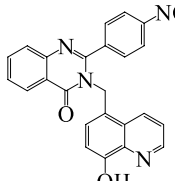
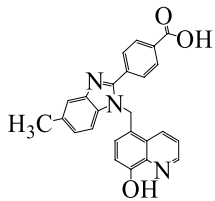
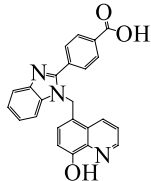
0.01 mol of *2-alkylbenzimidazoles* (**1** et **2**) is mixed with 0.02 mol of *5-chloromethyl 8-hydroxyquinoline hydrochloride* (**3**) in 50 mL of dimethylformamide (DMF), in the presence of 0.01 mol of potassium bicarbonate ( $\text{K}_2\text{CO}_3$ ). The reaction mixture is heated at 80 °C. The reaction is monitored by TLC, using a mixture of EtOH- $\text{CH}_2\text{Cl}_2$  (70:30) as eluent, and when the latter indicates the complete consumption of the starting products after 24 h, the reaction mixture is concentrated. To the rotary vacuum evaporator of the water pump, the residue thus obtained is hydrolyzed with 20 mL of water saturated with  $\text{NaHCO}_3$  and extracted with chloroform. The crude residue obtained is purified by chromatography on a column of silica gel, followed by recrystallization from EtOH-DMF (70:30).

The synthesis and characterization of compound **3** have been already published in another publication [23]. For the synthesis of the *benzimidazole* derivatives (**1** and **2**), we have followed a method already described in the literature [23] (Scheme 1).

### 2.3 Material and Electrolyte

The mild steel samples were used with C, 0.11; Si, 0.24; Mn, 0.47; Cr, 0.12; Mo, 0.02; Ni, 0.1; Al, 0.03; Cu, 0.14; Co, < 0.012; V, < 0.003; W, 0.06; Fe, balance, and the remainder of iron. Before any measurement, they were abraded with a series of emery paper grades 180–1200. The specimens are thoroughly washed with double distilled

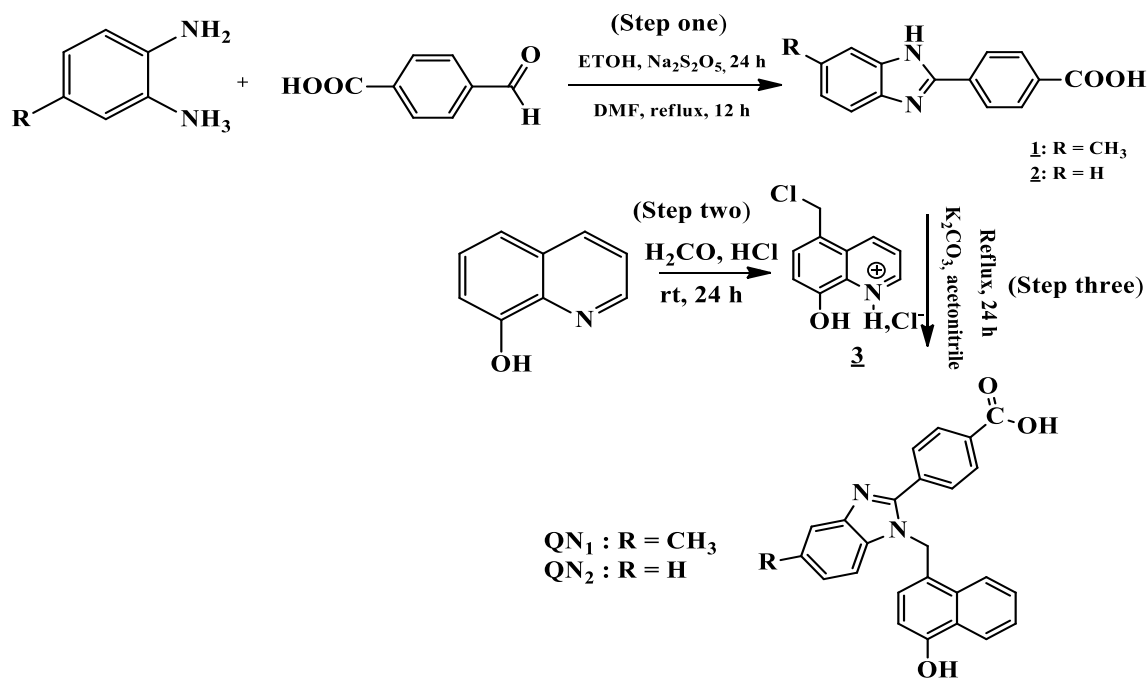
**Table 1** Percentage inhibition efficiency for different quinoline derivatives in 1.0 M HCl (the concentration used is  $10^{-3}$  M)

Quinoxaline derivative	Highest inhibition efficiency (%) <sup>(a)</sup>	Metal exposed	Reference
 (8-Hydroxyquinolin-5-yl) methyl 4-Chlorobenzoate	93.1	Mild steel	[21]
 (8-Hydroxyquinolin-5-yl) methyl 4-nitrobenzoate	90.1	Mild steel	[21]
 3-((8-hydroxyquinolin-5-yl)-methyl)-2-phenylquinazolin-4(3H)-one	94.4	Mild steel	[22]
 3-((8-hydroxyquinolin-5-yl)-2-(4-nitrophenyl)-quinazolin-4(3H)-one	95.9	Mild steel	[22]
 4-(1-((8-hydroxyquinolin-5-yl)methyl)-5-methyl-1H-benzimidazol-2-yl)benzoic acid (QN1)	97.4	Mild steel	This work
 4-(1-((8-hydroxyquinolin-5-yl)methyl)-1H-benzimidazol-2-yl)benzoic acid (QN2)	91.8	Mild steel	This work

<sup>(a)</sup>The inhibition efficiency values were determined using EIS measurements at 298 K after 1/2h of immersion.

<sup>(a)</sup>The inhibition efficiency values were determined using EIS measurements at 298 K after 1/2 h of immersion





**Scheme 1** Path of synthesis of QN1 and QN2

water, degreased with acetone and then dried [23]. The aggressive solution 1.0 M HCl was prepared by the dilution of concentrated HCl (37%) analytical grade with bi-distilled water. In this work, we tested these two synthesized compounds in corrosion inhibition in a concentration range from  $10^{-3}$  to  $10^{-6}$  M.

## 2.4 Electrochemical Study

Electrochemical study was realized in a three-electrode electrochemical cell, composed of a mild steel plate as a working electrode (with an exposed area of  $1 \text{ cm}^2$ ), a platinum counter-electrode and an SCE-saturated reference electrode. An electrochemical measurement has been taken using a potentiostat/Galvanostat/PGZ100 controlled by analysis software VoltaMaster4. Electrochemical experiments were analyzed using electrochemical software ORIGIN PRO 6.1. Electrochemical parameters were, then, extracted owing ZView software.

The potential intensity curves were obtained by using potentiodynamic polarization techniques with a scanning speed of  $30 \text{ mV min}^{-1}$ . Before polarization scans, the electrode was stabilized at OCP for 30 min. Inhibition efficiency was calculated by Eq. 1.

$$\eta_{\text{PDP}}(\%) = \left[ 1 - \frac{i}{i^0} \right] \times 100 \quad (1)$$

where ( $i$ ) and ( $i^0$ ) are the corrosion current density values with and without compounds.

The electrochemical impedance measurements (EIS) were taken on mild steel samples at constant potential (OCP) in the frequency range from 100 kHz to 100 mHz under potentiostatic conditions using an AC signal with amplitude of 10 mV peak to peak. The Boukamp program was used to analyze the results in terms of the equivalent electrical circuit.

The inhibition efficiency was calculated from the polarization resistance values by using the following relationship 2.

$$\eta_{\text{EIS}}(\%) = \frac{R_p - R_p^0}{R_p} \times 100 \quad (2)$$

where  $R_p^0$  and  $R_p$  are the polarization resistance in the absence and presence of the compounds.

## 2.5 Quantum Chemical Calculations and Monte Carlo Simulation

Quantum chemical calculations play a key role to predict the electronic properties and chemical behavior of organic compounds based on some intrinsic features from their molecular structure. Herein, we used the computational tools to back up the experimental inferences and establish a prediction correlation between the electronic structure properties, quantum chemical states and corrosion inhibition efficiency of the studied compounds. In the present theoretical work, we started with complete



geometry optimizations for the two compounds using density functional theory (DFT) with the 6-31G (d, p) basis set of atomic orbitals as implemented in the Gaussian 03 program package [24, 25]. Most of the molecular properties have been predicted from frontier molecular orbital (FMO) calculations that include highest occupied molecular orbital (HOMO), lowest unoccupied molecular orbital (LUMO) and energy gap ( $(\Delta E_{(LUMO-HOMO)})$ )

$$(\Delta E = E_{LUMO} - E_{HOMO}) \quad (3)$$

The fraction of electrons transferred ( $\Delta N_{FET}$ ) was calculated as follows:

$$\Delta N_{FET} = (\chi_{fe} - \chi_{inh}) / 2(\eta_{fe} - \eta_{inh}) \quad (4)$$

where  $\chi$  and  $\eta$  denote to electronegativity and hardness, respectively.

The Fukui indices on the backbone atoms have been also computed. As part of the computational framework study, the adsorption of compounds on the Fe surface was simulated by applying molecular dynamic approaches. The molecular adsorption was modeled in a simulation box of dimension  $24 \times 24 \times 42$  Å, constructed from supercell, constructed from supercell of 96 Fe atoms. The spatial coordinates of the Fe atoms at the bulk position were kept frozen, while all other surface atoms were set to relax on the geometry optimization course.

## 3 Results and Discussion

### 3.1 Chemical Study

#### 3.1.1 Chemical Data and Value

**3.1.1.1 Synthesis of 4-(6-Methyl-1H-benzo[d]imidazol-2-yl) benzoic Acid (QN1)** Yield % 60;  $M_p$  165 °C;  $F_r$  0.63; Aspect Brown solid; IR: 1794 (C=N), 1777 (C=C), 3641 (OH), 1905 (CH<sub>2</sub>). <sup>1</sup>H NMR,  $\delta_{ppm}$  4.64 (s, 2 H, CH<sub>2</sub>), 2.36–2.48 (DMSO-solvent), 3.25–3.43 (H<sub>2</sub>O), 4.68 (s, 1 H, OH), 2.05 (s, 3 H, CH<sub>3</sub>), 12.27 (s, 1 H, OH-carboxylic acid), 7.00–7.26–7.66–8.83–8.84 (m, 5 H, Ar<sub>quinoline</sub>) 7.42–7.44–7.53–8.393–8.42 (m, 7 H, ArH-benzimidazole). <sup>13</sup>C NMR  $\delta_{ppm}$  57.56 (CH<sub>2</sub>), 20.95 (CH<sub>3</sub>), 153.83 (ArC-OH<sub>quinoline</sub>), 159.63 (C=O Acid function), 155.39 (C-N), 115.67–122.12–126.88–128.29–129.02 (ArCH<sub>benzimidazole</sub>), 132.09–132.33–133.57–148.31–148.23 (ArC<sub>benzimidazole</sub>), 111.04–123.49–128.25–15.34 (ArCH<sub>quinoline</sub>), 127.73–129.74–139.30 (ArC-quinoline). **Analysis Elemental % Calculated:** C, 73.34; H, 4.68; N, 10.26. **Obtained % C,** 73.30; H, 4.66; N, 10.24.

**3.1.1.2 Synthesis of 4-(1H-benzo[d]imidazol-2-yl)benzoic Acid (QN2)** Yield % 80;  $M_p$  180 °C;  $F_r$  0.61; Aspect Brown solid; IR: 1798 (C=N), 1628 (C=C), 3325 (OH), 1873 (CH<sub>2</sub>), 2020 (C=O), <sup>1</sup>H NMR  $\delta_{ppm}$  5.78 (s, 2 H, CH<sub>2</sub>), 2.47–2.85 (DMSO-solvent), 3.44 (H<sub>2</sub>O), 13.25 (s, 1 H, OH<sub>carboxylic acid</sub>), 7.00–7.261–7.66–8.83–8.84 (m, 5 H, ArH), 7.42–7.44–7.53–8.39–8.42 (m, 8 H, ArH<sub>benzimidazole</sub>). <sup>13</sup>C NMR  $\delta_{ppm}$  47.67 (CH<sub>2</sub>), 148.44 (ArC-OH<sub>quinoline</sub>), 151.50 (C=O<sub>Acid function</sub>), 149.45 (C-N), 119.92–123.41–127.81–127.86 (ArCH<sub>benzimidazole</sub>), 136.44–136.35–144.71–147.35 (ArC<sub>benzimidazole</sub>), 112.27–120.28–126.68–136.50–148.21 (ArCH<sub>quinoline</sub>), 124.46–130.77–143.10 (ArC<sub>quinoline</sub>). **Analysis Elemental % Calculated** C, 72.90; H, 4.33; N, 10.63. **Obtained % C,** 74.50; H, 4.30; N, 10.66.

The IR spectra of the two compounds QN1 and QN2 show the main bands of elongation vibration characteristics of the functional groups, a very intense band around 2000 cm<sup>-1</sup> which corresponds to the asymmetric elongation vibration, a band is observed around 1500 cm<sup>-1</sup>, it is attributed to the vibration of the CH<sub>2</sub> group (the slope between the two functions), and finally an absorption band is observed around 36,009–3900 cm<sup>-1</sup> which characterizes the aromatic carboxylic acid function (Ar-COOH).

### 3.2 Proposal Mechanism

See Scheme 2.

### 3.3 Open Circuit Potential

Figure 1 presents the open circuit potential (OCP) versus time at different concentrations of inhibitors QN1 and QN2 at 298 K.

It is noted that the potential for blank solution stays stable with time. This phenomenon characterizes the corrosion of mild steel with a formation of corrosion products. So, in the presence of QN1 and QN2, the potential shift in the anodic direction and speedily declined and touched a steady rate after 200 s. The disbanding of oxide layer [26] and the adsorption particles on the substrate of MS are the foremost explanations for the detected OCP weakening [26].

### 3.4 Potentiodynamic Polarization Study

The curves of the potentiodynamic polarization of the M-steel in 1.0 M HCl with and without different concentrations of all compounds are shown in Fig. 2. The PDP considerations and the inhibition efficiency of both compounds are given in Table 2.

Figure 2 shows that the cathodic and anodic reactions are affected in the presence of QN1 and QN2. This implies that the presence of QN1 and QN2 in 1.0 M HCl solutions impedes the cathodic hydrogen evolution and anodic

**Scheme 2** Mechanism of N-alkylation of 5-chloromethyl-8-hydroxyquinoline hydrochloride by benzimidazole derivatives

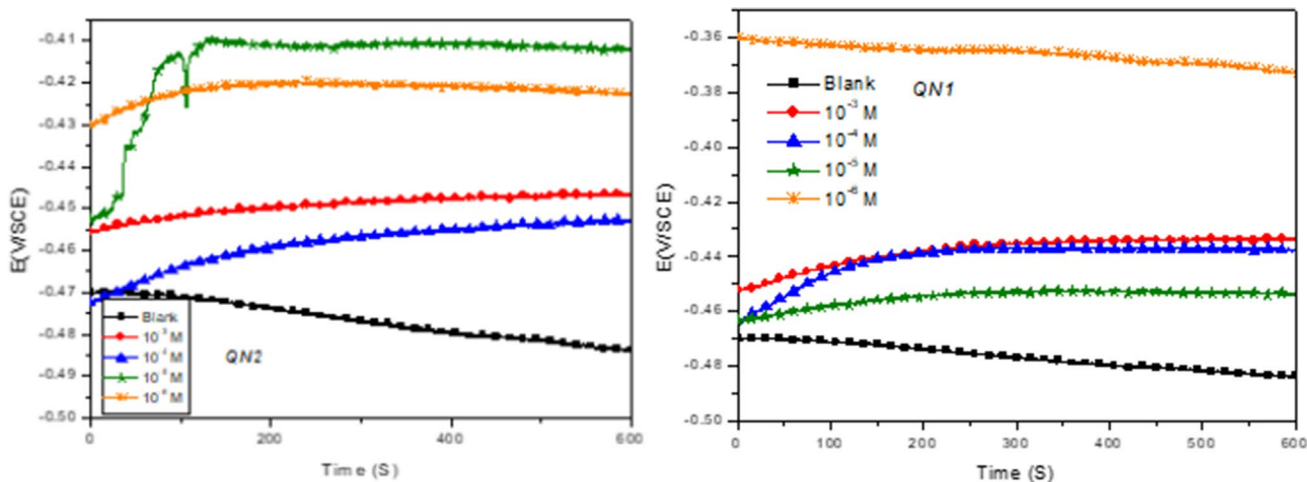
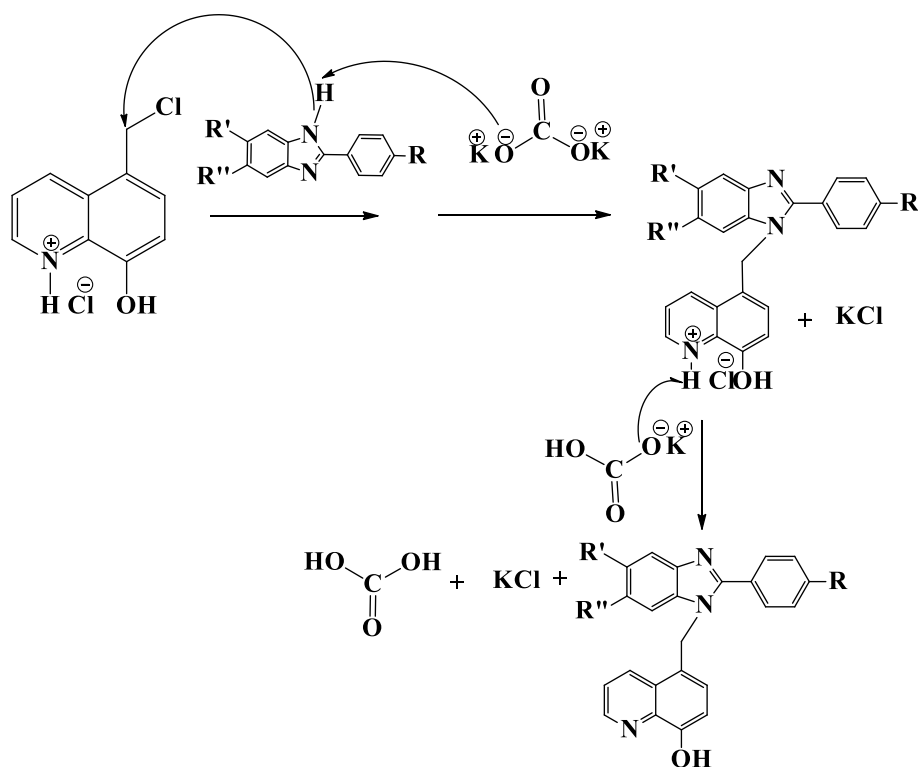


**Fig. 1** Evolution of open circuit potential (OCP) versus time for MS in 1.0 M HCl medium with and without the addition of QN1 and QN2 at 298 K

dissolution reaction of MS; this observation shows that QN1 and QN2 exhibit anodic and cathodic inhibition effects. QN1 and QN2 cause a notable decrease in current density and corrosion rate values. With the presence of QN1 and QN2, the cathodic/anodic polarization plots reveal that the curve shifted toward lower current density. This trend indicates that the steel surface active site was blocked owing to the QN1 and QN2 molecules adsorbed. Anodic and cathodic corrosion reactions of mild steel samples were significantly

inhibited by QN1 and QN2 which suggest QN1 and QN2 as a mixed type. The QN1 and QN2 adsorption on the mild steel surface possibly will not appreciably change the cathodic branch slope and shape, signifying that the hydrogen evolution mechanism does not change after inhibitor adsorption. Minor displacement in  $E_{\text{corr}}$  value to negative site (Table 2) was observed. In this way, if the corrosion potential displacement is superior than  $\pm 85$  mV compared to that of blank, the inhibitor may be observed as a cathodic or





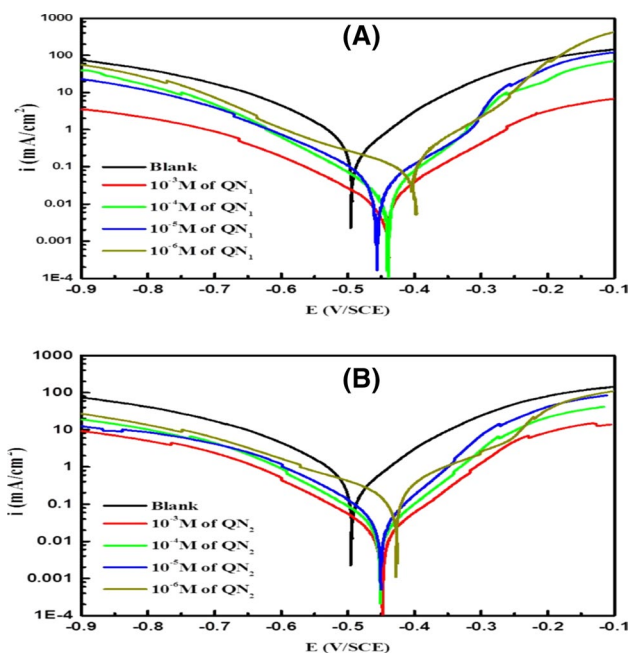


**Fig. 2** Potentiodynamic polarization curves of MS in 1.0 M HCl medium with and without the addition of **a** QN1 and **b** QN2 at 298 K

anodic type [27, 28]. Though the change in  $E_{corr}$  value with the sample without inhibitor is below 85 mV, confirming the mixed-type nature of QN1 and QN2.

It is very clear from the table that the presence of QN1 and QN2 in the 1.0 M HCl solution affects the Tafel slopes values. However, it is noticed that the change in  $\beta_c$  values of the inhibited systems with respect to that of the blank is independent of inhibitor concentration, that is, there is no pattern in  $\beta_c$  values of the inhibited solution with respect to that of the blank as the concentration of QN1 and QN2 is increased. This means that the kinetics of the cathodic reactions are not affected and the inhibition is by simple geometric blocking mechanism [29, 30]. On the contrary, a steady decrease in  $\beta_a$  value with increasing QN1 and QN2 concentration is observed. For instance, the presence of  $10^{-6}$  M QN1 and QN2 in the corrosive medium decreases the  $\beta_a$

value from 150 to 99 mV  $\text{dec}^{-1}$  for QN1 and to 77 mV  $\text{dec}^{-1}$  for QN2. When the concentration was raised to  $10^{-3}$  M, the  $\beta_a$  value further decreases to 86 mV  $\text{dec}^{-1}$  for QN1 and 71 mV  $\text{dec}^{-1}$  for QN2. This implies that the kinetics of the iron dissolution in 1.0 M HCl solution is modified during the inhibition process by these two compounds [31].

The  $i_{corr}$  was also observed to decrease when the inhibitor concentration increased, denoting more QN1 and QN2 molecules adsorption on the mild steel surface. The  $\eta_{PDP}(\%)$  increases with increasing compound concentrations and reaches an optimal value ranging from 97.7 to 91.6% at  $10^{-3}$  M for QN1 and QN2, respectively. It is also evident that the  $\eta_{PDP}(\%)$  followed the order QN1 > QN2. This result can be explained by the presence of the electron donor methyl group on the molecular structure of the compound QN1.

### 3.5 Electrochemical Impedance Measurements

The corrosion inhibition property of QN1 and QN2 on mild steel was also examined by electrochemical impedance spectroscopy (EIS) in order to confirm the above-obtained results and to study the inhibition mechanism in more details. Figure 3 presents the Nyquist diagrams of mild steel obtained at open circuit potential in 1.0 M HCl solution in the absence and presence of QN1 and QN2 at different concentrations after 30 min of immersion at 298 K. As shown in this figure, we remark that when QN1 and QN2 are added to the 1.0 M HCl solution, the size of the impedance diagram increases as the concentration rises and consequently the inhibitory efficacy increases, due to the adsorption of inhibitor molecules on the metal surface [32].

Examination of Fig. 3 reveals that each impedance diagram in the presence and the absence of QN1 and QN2 at different concentrations consists of a capacitive loop at high frequency (HF). The capacitive loop is usually associated with the single charge transfer process of the metal corrosion and double layer behavior [32]. The depressed semicircles are generally attributed to the frequency dispersion, arising from roughness and inhomogeneity of electrode surface [33]. So, in such cases an constant phase element (CPE)

**Table 2** Potentiodynamic polarization data's for mild steel in 1.0 M HCl with and without the different concentrations of inhibitors at 298 K

Medium	Conc. (M)	$E_{corr}$ (mV SCE)	$i$ ( $\mu\text{A cm}^{-2}$ )	$\beta_c$ (mV $\text{dec}^{-1}$ )	$\beta_a$ (mV $\text{dec}^{-1}$ )	$\eta_{PDP}$ (%)	$\theta$
HCl	1.0	-498	983	-140	150	-	-
	$10^{-3}$	-433	22	-133	86	97.7	0.977
QN1	$10^{-4}$	-439	31	-131	88	96.8	0.968
	$10^{-5}$	-456	32	-136	90	96.7	0.967
	$10^{-6}$	-394	60	-153	99	93.8	0.938
	$10^{-3}$	-446	82	-129	71	91.6	0.916
QN2	$10^{-4}$	-449	84	-134	72	91.4	0.914
	$10^{-5}$	-447	105	-130	74	89.3	0.893
	$10^{-6}$	-422	348	-147	77	64.6	0.646

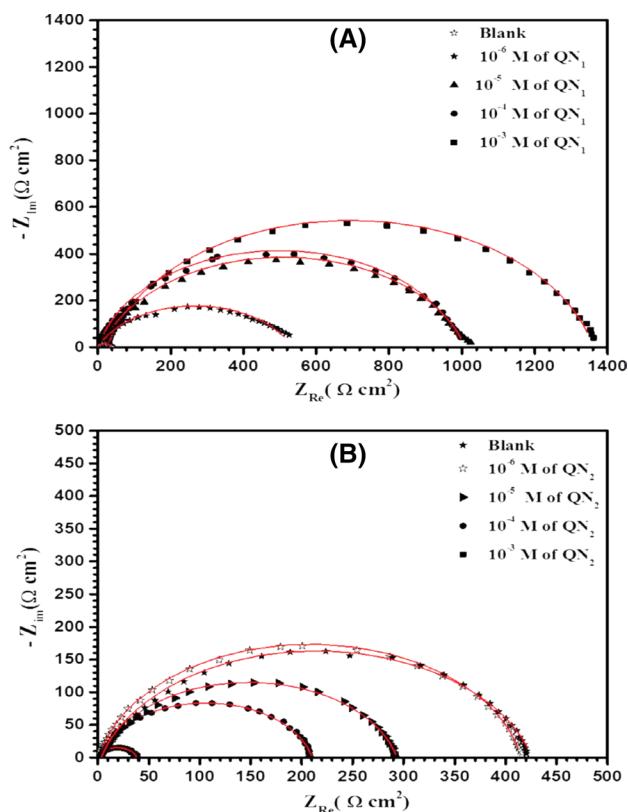


Fig. 3 Nyquist diagrams of steel in 1.0 M HCl with and without different concentrations of a QN1 and b QN2 at 298 K

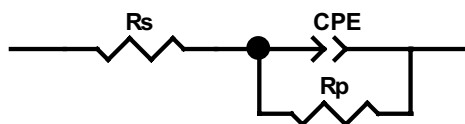


Fig. 4 Equivalent circuit corresponding to the impedance spectra

is used instead of a pure capacitor to compensate for non-ideal capacitive response of the interface to get a more fit of experimental data [34] and the impedance is given by Eq. 5:

$$Z_{CPE} = Q^{-1} (i\omega)^{-n} \tag{5}$$

where  $Q$  is proportionality coefficient (in  $\Omega^{-1} \text{sn cm}^{-2}$ ),  $\omega$  is the angular frequency and  $i$  is the imaginary number,  $n$  is the deviation parameter ( $-1 \leq n \leq +1$ ), has the meaning of a phase shift. While  $n=0$ , the CPE represents a pure resistor, for  $n=-1$  and inductor and for  $n=+1$ , a pure capacitor [35]. In this study, the best fit of the extracted experimental data is obtained for the equivalent circuit given in Fig. 4. Figure 4 shows the electrical equivalent circuit diagram to model mild steel/1.0 M HCl interface which consists of a CPE, polarization resistance ( $R_p$ ) and solution resistance ( $R_s$ ).

A constant phase element (CPE) is used instead of a pure capacitor to compensate for non-ideal capacitive response of the interface [36].  $R_p$  is corresponding to the corrosion reaction at a mild steel substrate/solution interface, whose value is a measure of electron transfer across the surface and is proportional to corrosion rate. It is clear that the measured impedance plots are in accordance with those calculated by the used equivalent circuit model. All the corresponding fitted parameters are listed in Table 3. The values of double layer capacitance ( $C_{dl}$ ) in the absence and presence of QN1 and QN2 were calculated using the following equation [37]:

$$C_{dl} = (QR_p^{1-n})^{1/n} \tag{6}$$

The capacitive behavior of mild steel in the presence of QN1 and QN2 could be visualized from Bode's plot (Fig. 5). A destructive outbreak of HCl acid corroded the mild steel and made the metal surface highly asymmetrical, which could be explained out by the small phase angle. On the contrary, adsorption of the inhibitors on mild steel surface effectively lowered surface irregularities; additionally, we address the evolution of phase angle by measuring their values at arbitrarily chosen frequency (100 Hz) (Fig. 5). Clearly, with increasing concentration of both inhibitors the phase angle values dramatically increase as

**Table 3** Impedance parameters and corrosion inhibition efficiency of mild steel in 1.0 M HCl at different inhibitor concentrations of QN1 and QN2

Medium	Conc. (M)	$R_s$ ( $\Omega \text{ cm}^2$ )	$R_p$ ( $\Omega \text{ cm}^2$ )	$C_{dl}$ ( $\mu\text{F cm}^{-2}$ )	$n$	$Q$ ( $\mu\text{F Sn}^{-1}$ )	$\eta_{EIS}$ (%)
HCl	1	1.12	34.7	121	0.773	419.0	–
	$10^{-3}$	2.75	1332	34	0.873	56.45	97.4
QN1	$10^{-4}$	3.30	998	39	0.887	79.57	96.5
	$10^{-5}$	1.15	996	58	0.839	59.00	96.5
	$10^{-6}$	3.00	534	124	0.746	247.0	93.5
	$10^{-3}$	3.75	422	70	0.839	123.0	91.8
QN2	$10^{-4}$	1.69	413	55	0.889	130.0	91.6
	$10^{-5}$	2.70	290	50	0.853	93.50	88.1
	$10^{-6}$	1.23	209	91	0.859	103.0	83.5



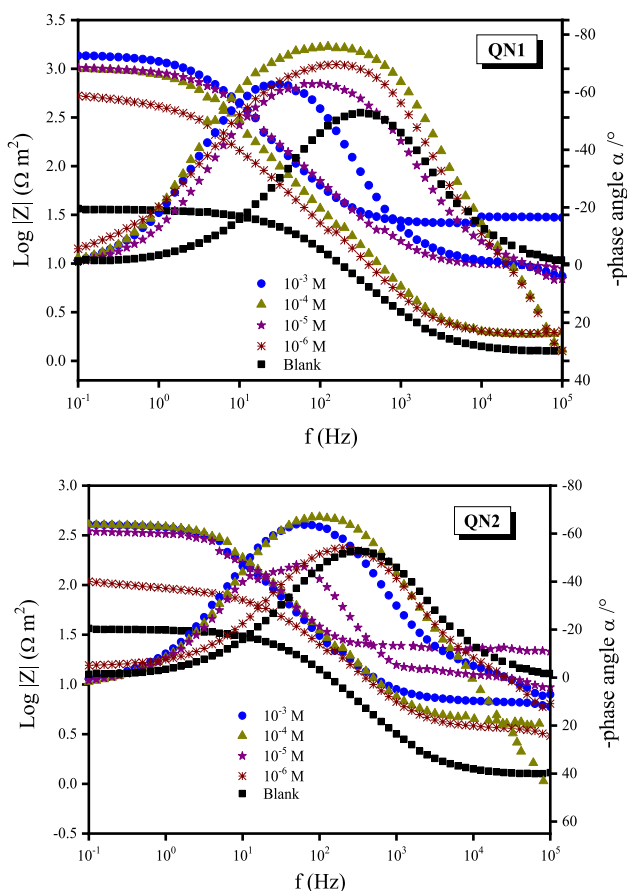


**Fig. 5** Bode’s plots and Phase angle values for mild steel in 1.0 M HCl solution with and without different concentrations of QN1 and QN2 at 298 K

well. Furthermore, whatever the concentration used, the phase angle values are higher than that of the blank, which also describes the non-ideal capacitor [38]. This indicates an increased capacitance of the interference due to the presence of adsorbed inhibitors molecules at the interface [38]. Indeed, only one time constant is detected on the Bode diagram without and with various concentrations of QN1 and QN2.

Analysis of the impedance results in Table 3 shows that the polarization resistance value,  $R_p$ , increases with the concentration of QN1 and QN2 and reaches a maximum value 1 mM. The increase in  $R_p$  values demonstrates the improved protective effect of those compounds, and a slow corroding system, due to the gradual replacement of water molecules by QN1 and QN2 molecules on the surface and consequently to a decrease in the number of active sites necessary for the corrosion reaction [39]. In addition, the adsorption of both compounds on the steel surface was confirmed by decreases in double layer ( $C_{dl}$ ) capacity values at different concentrations [39]. This decrease of  $C_{dl}$  with concentrations can be explained by a decrease in the local dielectric constant and/

or an increase in the protective layer thickness on the electrode surface. This trend is in accordance with Helmholtz model, given by the following equation.

$$C_{dl} = \frac{\epsilon_0 \times \epsilon}{e} \times S \tag{7}$$

where  $\epsilon$  is the dielectric constant of the protective layer,  $\epsilon_0$  is the permittivity of free space ( $8.854 \times 10^{-14} \text{ F cm}^{-1}$ ) and  $S$  is the effective surface area of the electrode. It is worth pointing that the rise in the deviation parameter ( $n$ ) values after the inhibitors addition, which can be related to a decrease in surface inhomogeneities caused by adsorption of the QN1 and QN2 molecules on mild steel surface [40].

### 3.6 Temperature Effect and Kinetic Activation Parameters

The temperature has been instrumental in our understanding and approach to study the corrosion of steel. Also, to calculate the thermodynamic parameters of activations [41], the temperature parameters are given in Table 4 and Fig. 6.

The activation parameters we were aiming in our work:

The activation energy ( $E_a$ ) which is calculated by the Arrhenius equation (Eq. 8, Fig. 7):

$$i_{corr} = A \exp\left(\frac{-E_a}{RT}\right) \tag{8}$$

$E_a$  activation energy of the reaction,  $R$  constant perfect gas ( $8.314 \text{ J mol}^{-1} \text{ K}^{-1}$ ), a preexponential factor,  $T$  temperature in Kelvin.

The activation enthalpy ( $\Delta H_a$ ) and the entropy activation ( $\Delta S_a$ ) that they are calculated by the extrapolation of the Arrhenius equation (Eq. 9, Fig. 8):

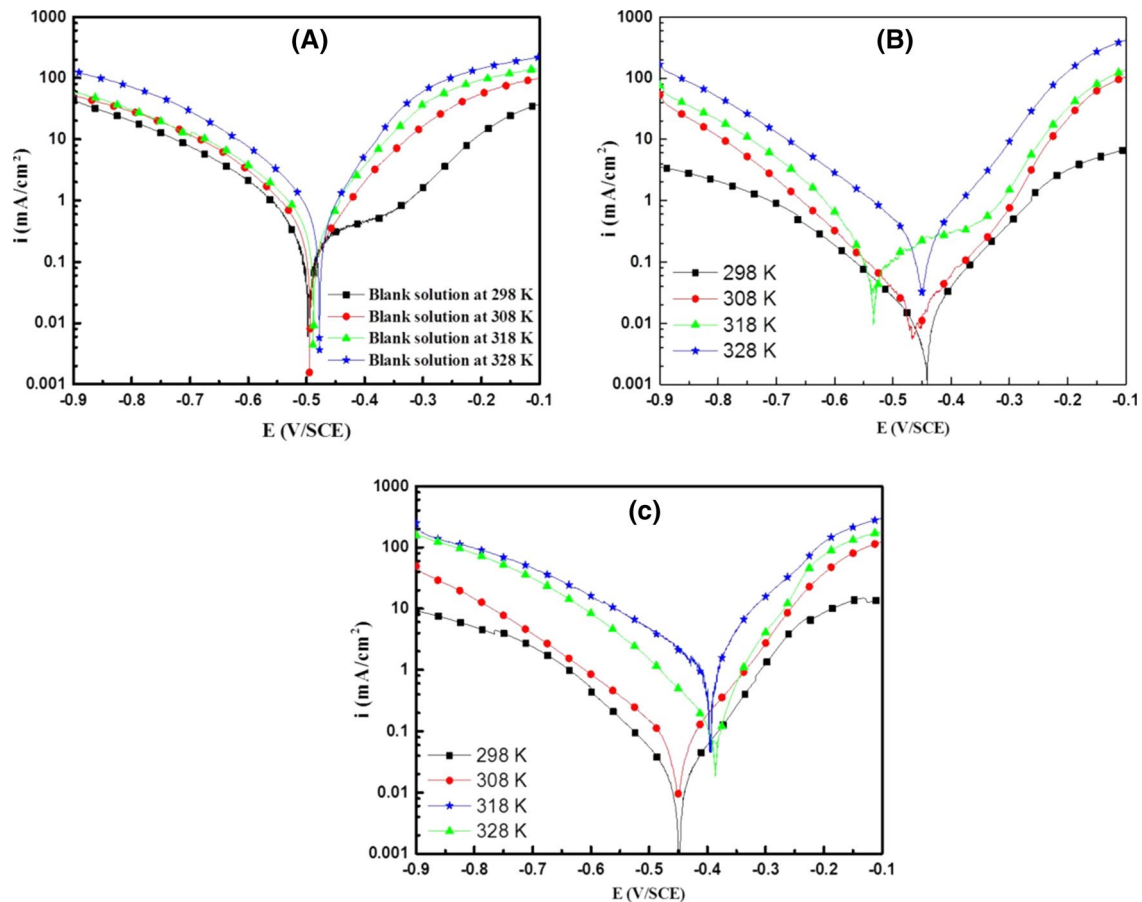
$$i_{corr} = \frac{RT}{Nh} \exp\left(\frac{\Delta S_a}{R}\right) \exp\left(\frac{-\Delta H_a}{RT}\right) \tag{9}$$

where  $N$  and  $h$  are the Avogadro’s and the Plank’s constants, respectively.

From Table 4, we can see that the increase in temperature did not significantly affect the values of the inhibitory efficiencies, so it can be said that our compounds are resistant to the corrosion of high-temperature steel. Therefore, these two compounds are profitable on an industrial scale for example in stripping baths. Always in Table 4, the activation energy value of the blank solution ( $E_a$ ) reported significantly less than the other two compounds (QN1 and QN2). In light of this result, it can be said that the addition of the two compounds caused the birth of the energy barriers resulting by the interaction of the system; inhibitor/substrate/1.0 M HCl. This says that our compounds are adsorbed on the surface of the steel [42]. In this study, the corrosion reaction is spontaneous that appear

**Table 4** Evolution of the temperature and the activation parameters for M-steel in 1.0 M HCl in the presence of  $10^{-3}$  M of QN1 and QN2

Temp (K)	$E_{\text{corr}}$ (mV SCE $^{-1}$ )	$i$ ( $\mu\text{A cm}^{-2}$ )	$\beta_a$ (mV dec $^{-1}$ )	$B_c$ (mV dec $^{-1}$ )	$\eta_{\text{PDP}}$ (%)	$E_a$ (KJ mol $^{-1}$ )	$\Delta H_a$ (KJ mol $^{-1}$ )	$\Delta S_a$ (J mol $^{-1}$ K $^{-1}$ )
<i>Blank</i>								
298 $\pm$ 2	-498	983	150	-140	-	21	18.5	-126
308 $\pm$ 2	-491	1200	184	-112	-			
318 $\pm$ 2	-475	1450	71	-124	-			
328 $\pm$ 2	-465	2200	161	-118	-			
<i>QN1</i>								
298 $\pm$ 2	-433	22	86	-133	97.7	52.55	49.96	-51.3
308 $\pm$ 2	-457	48	110	-98	96.0			
318 $\pm$ 2	-532	83	84	-105	94.7			
328 $\pm$ 2	-442	158	130	-84	92.8			
<i>QN2</i>								
298 $\pm$ 2	-446	82	75	-129	91.6	34.83	32.23	-100.3
308 $\pm$ 2	-445	127	131	-97	89.4			
318 $\pm$ 2	-390	176	131	-73	87.8			
328 $\pm$ 2	-397	308	178	-81	86.0			

**Fig. 6** Effect of temperature on the polarization curves of **a** mild steel in 1.0 M HCl and in the presence of **b** QN1 and **c** QN2

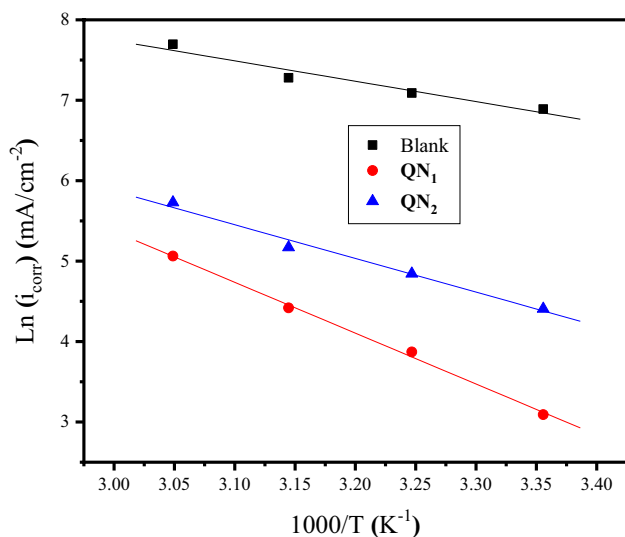


**Fig. 7** Arrhenius lines calculated from the polarization curves of mild steel in 1.0 M HCl with and without the addition of inhibitors at different temperatures

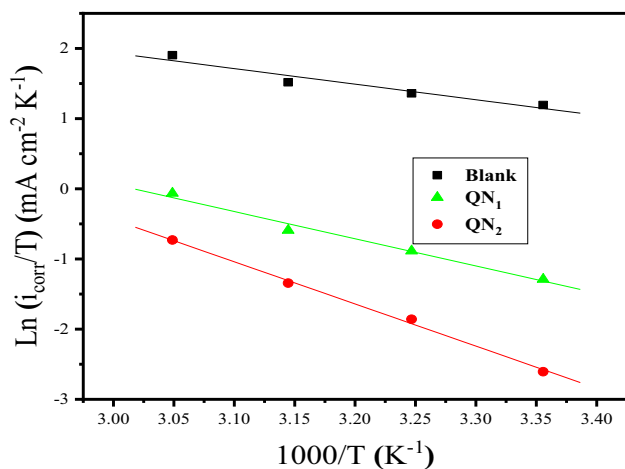


**Fig. 8** Variation of  $\text{Ln}(i_{\text{corr}}/T)$  versus  $1000/T$  in 1.0 M HCl with and without the addition of inhibitors at different temperatures

by the positive values of the activation enthalpy ( $\Delta H_a$ ) in the absence and in the presence of the compounds QN1 and QN2. The spontaneity of reaction has an advantage of minimizing energy [43]. The increase of  $\Delta S_{ac}$  value in the inhibited media compared to the uninhibited which implies that a rise in the disordering of the inhibited electrolyte [43].

In this work, the temperature parameters show that our N-heterocyclic compounds are profitable at high temperatures. However, the activation parameters also show that our compounds are very adsorbed on the surface of the steel in 1.0 M HCl.

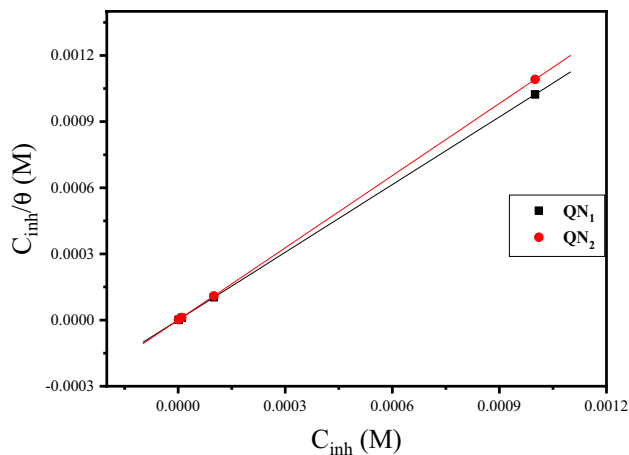


**Fig. 9** Langmuir adsorption isotherm of inhibitors on the surface of mild steel in HCl at 298 K

**Table 5** Adsorption parameters calculated for inhibitors from the Langmuir isotherm

Inhibitors	$K_{\text{ads}}$ ( $\text{L mol}^{-1}$ )	$R^2$	$\Delta G_{\text{ads}}^\circ$ ( $\text{KJ mol}^{-1}$ )
QN1	$0.27 \times 10^7$	0.9999	-46.70
QN2	$2.93 \times 10^7$	0.9999	-46.85

### 3.7 Thermodynamic Parameters of Adsorption

In particular, the thermodynamic parameters of adsorption are a dominant feature in the field of corrosion of steels to understand the mechanism of interaction between inhibitors and the surface of steel [44]. One of the thermodynamic parameters we have been interested in this work is the adsorption energy ( $\Delta G_{\text{ads}}^\circ$ ). The adsorption energy ( $\Delta G_{\text{ads}}^\circ$ ) is calculated following Eqs. (10, 11) [44]:

$$\frac{C}{\theta} = \frac{1}{K_{\text{ads}}} + C \tag{10}$$

$$\Delta G_{\text{ads}}^\circ = -RTL \ln(K_{\text{ads}} \times C_{\text{ads}}) \tag{11}$$

In this study, we try several adsorption isotherms and we found that the best isotherm is Langmuir isotherm {(The preexponential factor  $R^2$  is close to unity (Fig. 9))}. The obtained isothermal data are shown in Table 5.

According to the literature, based on adsorption energy ( $\Delta G_{\text{ads}}^\circ$ ) values have concluded the type of adsorption (physisorption or chemisorption) [45]. In our case, the adsorption energy ( $\Delta G_{\text{ads}}^\circ$ ) values are lower than  $-40 \text{ kJ mol}^{-1}$  for two compounds QN1 and QN2. This shows that our compounds have much better adsorbed on the surface of the M-steel (MS) by chemical bonds (chemisorption), which justifies the good resistance to high temperature.

### 3.8 UV–Visible Spectroscopy

The UV–visible spectrometry is used in several important areas of study, based on the maximum wavelength [46]. In our case, we used UV–visible (UV–Vis) to confirm the complexing property of our compounds with M-steel in molar HCl. The observation of Fig. 10a, b shows that the maximum wavelengths ( $\lambda_{\max}$ ) have a displacement in the case of adding the two inhibitors of 285.81 at 254.42 nm for the compound QN1 (Fig. 10a) and 251.91 at 256.37 nm for the compound QN2 (Fig. 10b). These data show that our compounds have a good complexing property with iron ions, which confirms the good inhibitory efficiency (97% for the compound QN1).

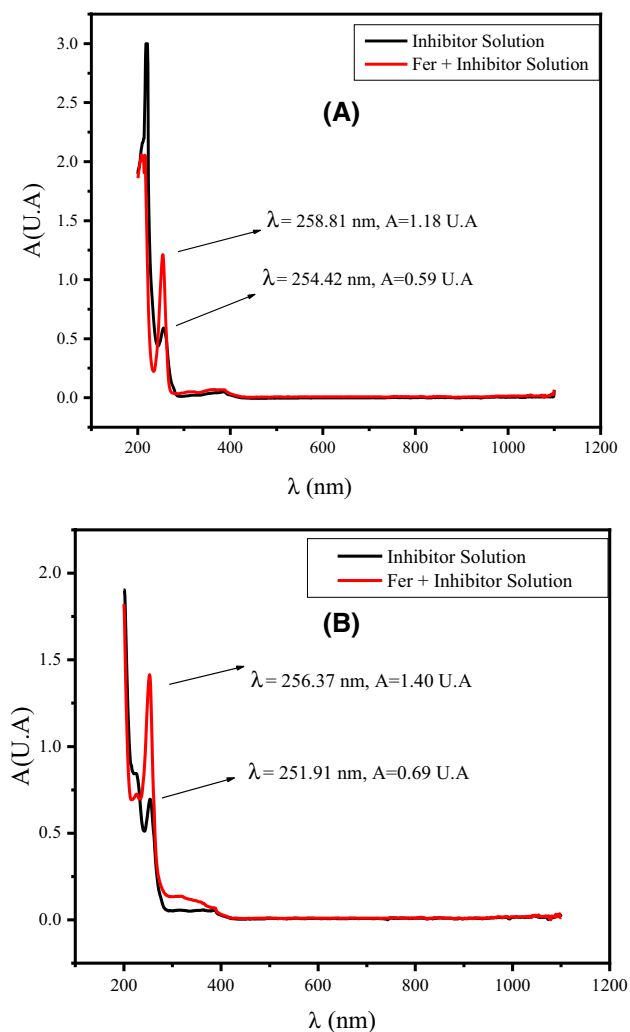


**Fig. 10** UV-visible spectra of 1.0 M HCl solution containing  $10^{-3}$  M of **a** QN1 and **b** QN2 before and after 6 h of mild steel immersion

### 3.9 SEM/EDAX

The role of electronic scanning microscope in surface characterization of steels has received increased attention across a number of disciplines in recent years [47]. The observation of surface image in HCl alone (Fig. 11c) shows that the surface was destroyed by corrosion. However, after the addition of the N-heterocyclic compounds QN1 and QN2 (Fig. 11a, b) in the corrosive solution, the surface of M-steel was protected by the layers of the organic compounds. The analysis by the scanning electron microscope confirms the inhibitory effect of these two compounds; thus, the SEM shows that both compounds are very adsorbed on the surface of the M-steel. This is in good agreement with the president studies. In addition, the elemental analyses obtained by EDAX analysis show that the heteroatoms such as N and O present in the molecules QN1 and QN2 are in contact with the MS surface and could serve as adsorption sites. This confirms the better adsorption of the two compounds on the surface of the steel [47].

### 3.10 Theoretical Calculations (DFT)

It is well established that the  $E_{\text{HOMO}}$  is connected to the capacity of molecule to donate electrons, which commonly refers to as ionization potential. The higher the  $E_{\text{HOMO}}$ , the higher the ability of compound electrons to the good electron acceptor [19]. On the other side, the  $E_{\text{LUMO}}$  is related to the electron-accepting capability of the compound, which commonly refers to as electron affinity [19]. The lower the  $E_{\text{LUMO}}$ , the greater the ability of compounds to accept electron in chemical interaction [19]. A potential inhibitor is the one with combined electronic properties features, having higher  $E_{\text{HOMO}}$  to contribute the electrons toward the empty d-orbital of the corroding metal and lower  $E_{\text{LUMO}}$  value to accept the electrons transferred from the Fe surface, furthermore, when the energy gap  $\Delta E$  is at minimum, since smaller values of the  $\Delta E$  coincides with greater inhibition effect of the molecule. The most relevant quantum chemical parameters such as  $E_{\text{HOMO}}$ ,  $E_{\text{LUMO}}$ ,  $\Delta E$  and  $\Delta N$  values were calculated and are presented in Table 6. In the present study, we aimed to carry out experimental and modeling studies and explore the effect of molecular surface on the inhibition performance of the inhibitor molecules. The optimized compound structure with HOMO and LUMO maps is shown in Fig. 12.

In this search, the introduction of  $-\text{CH}_3$  group in the molecular structure moiety as in QN1 has a significant effect to increase the electron donating ability of molecules [48]. This can be indicated from the higher value of  $E_{\text{HOMO}}$  compared to its counterpart QN2 with hydrogen. It is found that QN1 also has lower  $E_{\text{LUMO}}$  indicating the higher capacity to accept electron than QN2, and this is always required

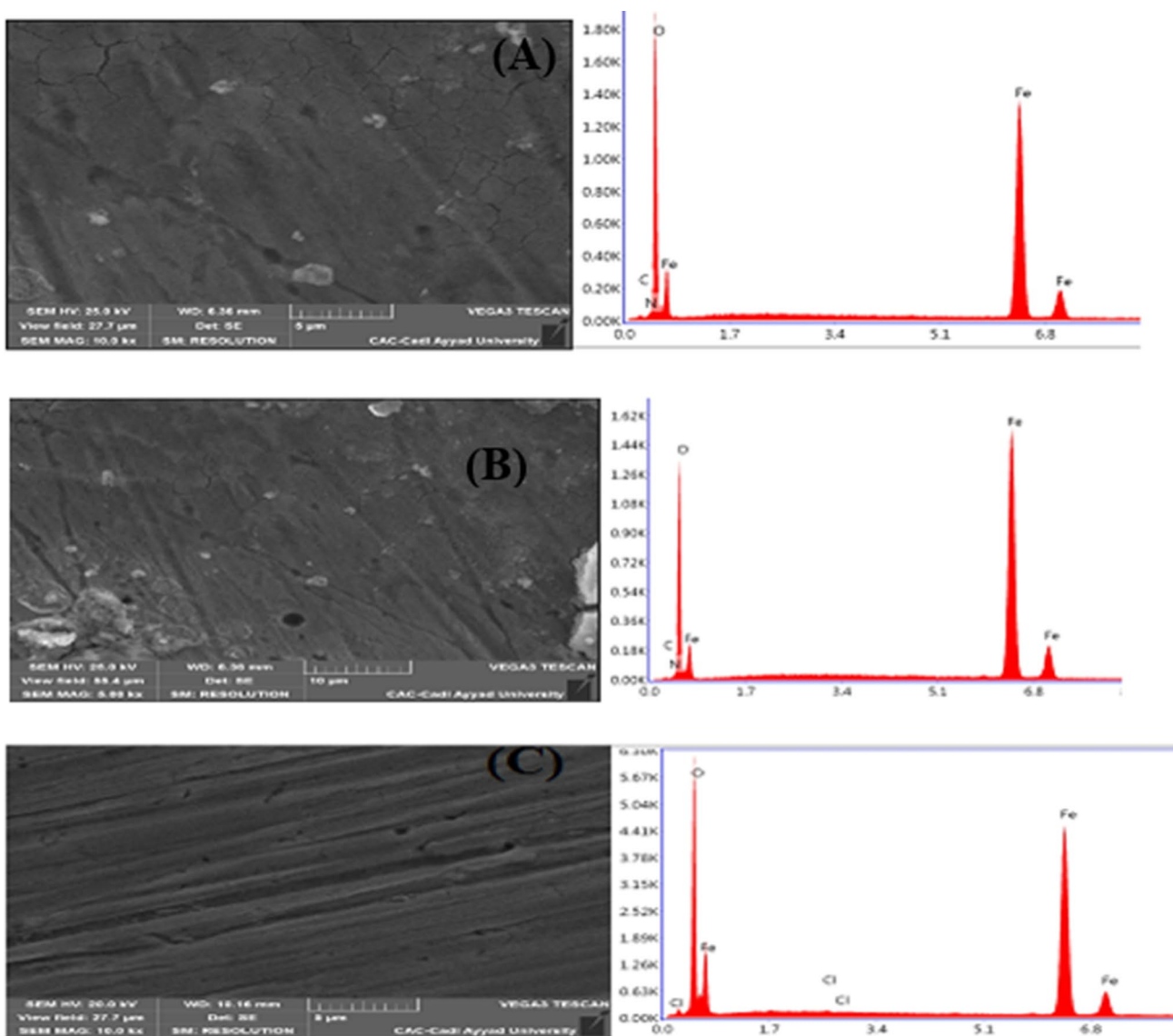


Fig. 11 Surface analysis of M-steel before (c) and after (a, b) submersion for 6 h in 1.0 M HCl with  $10^{-3}$  M of QN1 and QN2, respectively

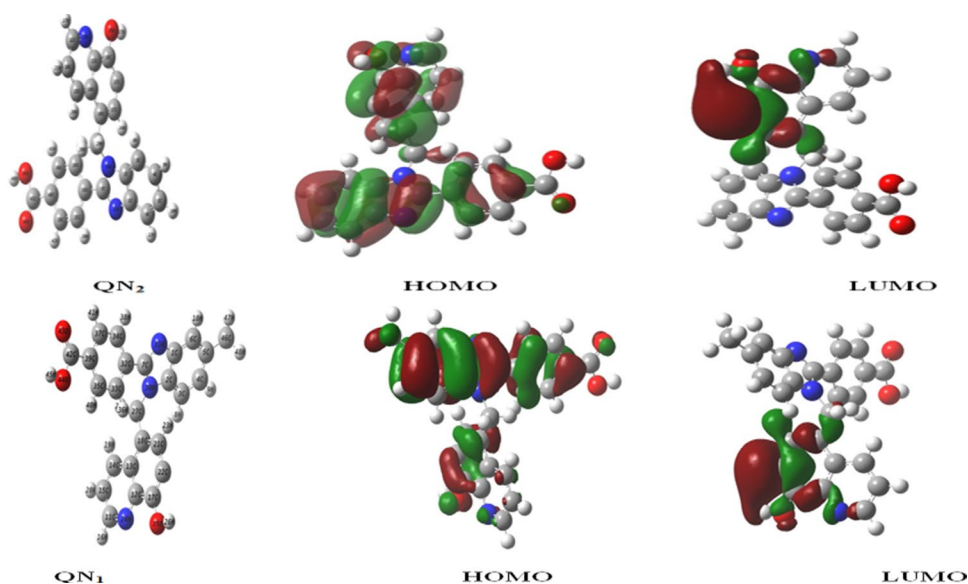
**Table 6** Quantum chemical parameters of compounds QN1 and QN2

Parameter	QN1	QN2
$E_{LUMO}$ (eV)	-2.936	-2.924
$E_{HOMO}$ (eV)	-5.910	-6.002
$\Delta E$ (eV)	2.974	3.078
$\Delta N$	1.854	1.660
%IE <sub>PDP</sub>	97.7	91.6

feature of organic compounds in chemical interaction like in our case adsorption. The gap energy of QN1 is lower than in QN2, which is considered an important structure stability index of compounds. Usually, softer molecules have smaller  $\Delta E$  signifying greater polarizability of compounds, which is another important feature of promising corrosion inhibitor. Another important parameter is the  $\Delta N$  value which describes the inhibition due to electron donations [48]. It is accepted that when  $\Delta N < 3.6$ , the inhibition effectiveness



**Fig. 12** Optimized molecular structures, HOMO and LUMO orbitals of molecules obtained by using DFT/B3LYP/6-31 G (d, p). Oxygen O is shown in red color and nitrogen N is in blue color



increases with enhancing donation–electron ability to the Fe surface of Fe. The  $\Delta N$  of QN1 is higher than QN2 which indicated that more electron can transfer from HOMO to d-orbitals of Fe surface. This inference further substantiates the experimental conclusions.

The susceptibility of molecule for polarization in the presence of an external electric field can be described by Fukui indices. Fukui indices (Table 7) provide insightful inference into the reactive atomic sites on inhibitor molecule structure. The  $f^+$ , denoted to the change in the electronic density when a molecule accept charge indicating the molecular reactivity toward nucleophilic attack. Accordingly, the highest value of  $f^+$  represents a preferred site for nucleophilic attack, whereas  $f^-$  corresponds to the reactivity of atoms toward the electrophilic attack when the molecule releases electrons. The highest value of  $f^-$  is associated with electrophilic attack. Table 7 lists the atomic sites that is likely act as nucleophilic sites and other atoms that can serve as electrophilic sites.

### 3.11 Monte Carlo Simulation

Metropolis Monte Carlo simulation method is a powerful technique used to better characterize the surface–adsorbate interaction identifying the favorable lowest energy adsorption configurations for the adsorbate components on Fe surface [25].

The top and side views of the most stable adsorption configurations of QN1 and QN2 on Fe (110) surface using Monte Carlo simulations are shown in Fig. 13.

It appears from Fig. 13 that QN1 and QN2 molecules are adsorbed in a flat parallel orientation so that the heteroatoms of each moiety of the molecule could interact with the iron surface. However, the methyl(–CH<sub>3</sub>) substituent at position 12 of QN1 molecule is adsorbed in a similar parallel mode which enhances the parallel adsorption orientation on the iron surface, while the benzene ring system adsorbed a perpendicular orientation on the iron surface, this increases the surface coverage and ensures strong interaction, and therefore, a high inhibition effect is observed experimentally [25]. The outputs and descriptors estimated by the Monte Carlo simulation, such as the total adsorption, rigid adsorption and deformation energies, are listed in Table 8.

The absorption energy is one of the most important parameters for adsorption; it is attributed to the energy released when the adsorbed adsorbate components are relaxed on the metal surface. The adsorption energy is defined as the sum of rigid adsorption and deformation energies of the adsorbate component. More negative adsorption energy value attributes to a big stabilized and strong interaction between adsorbed molecules and metal. Another parameter  $dE_{ad}/dN_i$  has been reported in Table 8, which is corresponding to the energy of substrate–adsorbate configurations where one of the adsorbate components has been removed [49]. As can be seen from the data in table that the negative values of adsorption energies of QN1 and QN2 on the Fe(110) surface are classified in the following order: QN1 < QN2 which is in good agreement with the experimental inhibition efficiency values.





**Table 7** Fukui indices for the nucleophilic and electrophilic attacks of QN1 and QN2 calculated using the DFT method

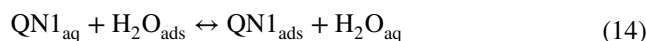
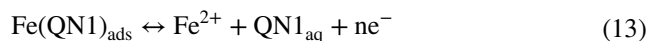
Atoms	QN2		QN1	
	$f_k^+$	$f_k^-$	$f_k^+$	$f_k^-$
C1	0.00988	-0.00833	-0.03746	-0.00629
C2	-0.00937	0.00614	-0.04292	<b>0.01722</b>
C3	-0.02408	0.00237	-0.00579	0.00398
C4	-0.07651	-0.01643	-0.03728	-0.01015
C5	<b>0.01074</b>	-0.02405	-0.07261	-0.02201
C6	-0.08261	-0.00090	-0.00758	-0.00803
C7	-0.0111	-0.02134	-0.0344	-0.00280
C12	-0.02544	-0.03352	-0.02715	-0.04659
C13	-0.01262	0.00104	-0.01419	-0.01266
C14	-0.00419	-0.03211	-0.00284	-0.02699
C15	-0.01055	-0.00992	-0.01235	-0.01359
C16	-0.03094	-0.03727	-0.02794	-0.03997
C18	-0.0032	<b>0.01998</b>	-0.02327	<b>0.04229</b>
C19	-0.02344	-0.02242	-0.03511	-0.0432
C22	<b>0.02107</b>	<b>0.04348</b>	-0.00235	<b>0.04555</b>
C23	-0.1639	-0.40157	-0.11211	-0.42961
N25	-0.04858	-0.02023	-0.04273	<b>0.07045</b>
O26	-0.02542	-0.0421	-0.04053	-0.03364
C28	-0.12817	<b>0.13201</b>	0.00662	0.00464
N31	-0.05152	<b>0.05308</b>	-0.02335	<b>0.01191</b>
N32	-0.09919	-0.02229	-0.02068	-0.02515
C33	0.00719	-0.01444	<b>0.01277</b>	-0.01503
C35	-0.05271	<b>0.02526</b>	-0.0063	0.00770
C36	-0.01159	-0.00326	-0.02328	-0.01022
C38	-0.01762	-0.01284	-0.00556	-0.01005
C40	-0.03665	-0.03528	-0.00603	-0.02000
C43	<b>0.01253</b>	-0.01801	-0.04313	-0.02152
O44	-0.03191	-0.03383	0.00607	-0.00969
O45	-0.01505	<b>0.00631</b>	-0.02965	-0.03123
C46			-0.00375	-0.00283

### 3.12 Corrosion Protection Mechanism

The corrosion inhibitor could be adsorbed on the mild steel surface and form a protective layer to improve the corrosion impedance of mild steel by decreasing the corrosion rate [50]. In general, the inhibitive mechanism is one of three approaches: (1) the chemical approach (chemisorption), where the inhibitor molecules are adsorbed on the metal surface and form a protective film; (2) the inhibitor molecules lead to the

formation of a protective layer through oxide protection of the base metal; and (3) the inhibitor molecules react with the potential corrosive components of the environment and form metal complexes [50].

The adsorption of QN1 and QN2 on mild steel can be clearly defined by considering the chemisorption processes (according to Sect. 3.7). The specific mechanism of corrosion inhibition of QN1 or QN2 to the surface of mild steel coupons is detailed in the following equations:



The chemisorption of QN1 or QN2 on mild steel is denoted by the donor–acceptor interactions between the lone pair of the electron from the carbonyl and amine groups of QN1 or QN2 with the *d*-orbitals of Fe. The value of free energy from the QN1 or QN2 adsorption was  $-46 \text{ kJ mol}^{-1}$ . This confirms that the adsorption mechanism of the QN1 or QN2 on the surface of the mild steel coupon was chemically adsorbed. The inhibition of corrosion begins by the displacement of water molecules by the inhibitor's capacity toward specific adsorption of the inhibitor on the metal's surface [51].

## 4 Conclusion

In this study, the results of experimental and theoretical studies show that N-heterocyclic compounds QN1 and QN2 have good corrosion inhibiting efficiencies of mild steel in the 1.0 M HCl solution. The polarization studies have shown that the studied inhibitors work as a mixed-type inhibitor with anodic predominance. The adsorption of the inhibitors on the mild steel surface obeys the Langmuir adsorption isotherm. The MC simulations and DFT calculations give a better overview on the reactivity of tested N-heterocyclic compounds QN1 and QN2 toward mild steel showing good correlation with the experimental results. The UV–visible spectrometry (UV–Vis) and scanning electron microscopy (SEM) confirm the adsorption effect of both inhibitors on the surface of the M-steel.



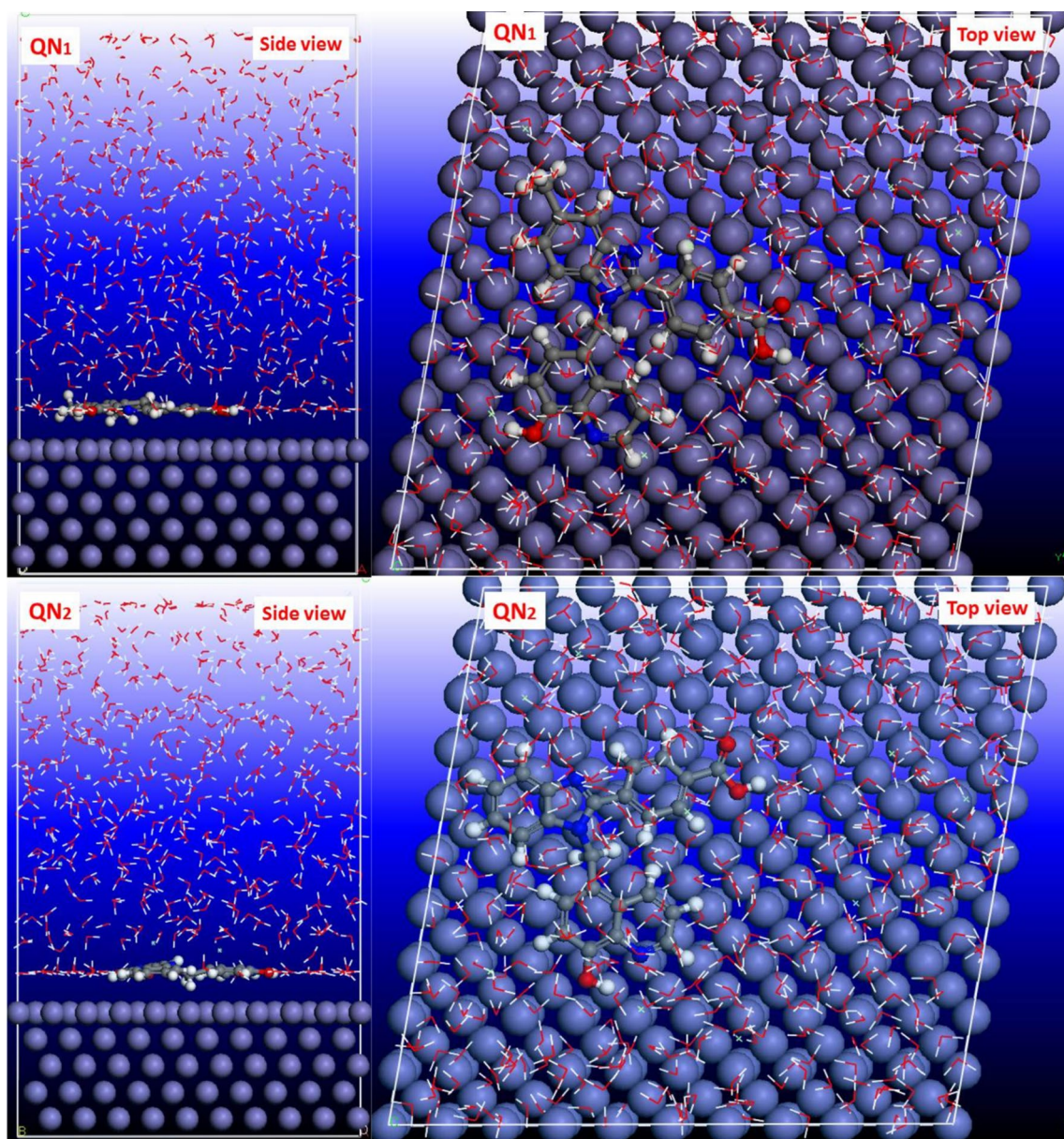


Fig. 13 Equilibrium configuration of inhibitors in aqueous systems obtained by MC simulations

**Table 8** Selected energy parameters obtained from MD simulations for adsorption of inhibitors on Fe (110) surface

System	$E_{\text{interaction}}$ (kJ mol <sup>-1</sup> )	$E_{\text{binding}}$ (kJ mol <sup>-1</sup> )
Fe(110) + QN1	- 867.12	867.12
Fe(110) + QN2	- 789.96	789.96

## References

1. Bentiss, F.; Traisnel, M.; Lagrenee, M.: The substituted 1,3,4-oxadiazoles: a new class of corrosion inhibitors of mild steel in acidic media. *Corros. Sci.* **42**, 127–146 (2000)
2. Bentiss, F.; Lagrenee, M.; Traisnel, M.; Hornez, J.C.: The corrosion inhibition of mild steel in acidic media by a new triazole derivative. *Corros. Sci.* **41**, 789–803 (1999)



3. Gvrten, A.: Adsorption behavior and inhibition corrosion effect of sodium carboxymethyl cellulose on mild steel in acidic medium. *Acta Phys. Chim Sin.* **24**, 2236–2242 (2008)
4. Darband, G.B.; Aliofkhaezaei, M.; Khorsand, S.; Sokhanvar, S.; Kaboli, A.: Science and engineering of superhydrophobic surfaces: review of corrosion resistance, chemical and mechanical stability. *Arab. J. Chem.* **13**, 1763–1802 (2020)
5. Zarrouk, A.; Zarrok, H.; Ramli, Y.; Bouachrine, M.; Hammouti, B.; Sahibed-dine, A.; Bentiss, F.: Inhibitive properties, adsorption and theoretical study of 3,7-dimethyl-1-(prop-2-yn-1-yl)quinoxalin-2(1H)-one as efficient corrosion inhibitor for carbon steel in hydrochloric acid solution. *J. Mol. Liq.* **222**, 239–252 (2016)
6. Kannan, P.; Rao, T.S.; Rajendran, N.: Improvement in the corrosion resistance of carbon steel in acidic condition using naphthalen-2-yl-naphthalene-2-carboxamide inhibitor. *J. Colloid Interface Sci.* **512**, 618–628 (2018)
7. Houslay, M.D.; Ellory, J.C.; Smith, G.A.; Hesketh, T.R.; Stein, J.M.; Warren, G.B.; Metcalfe, J.C.: Exchange of partners in glucagon receptor-adenylate cyclase complexes. Physical evidence for the independent, mobile receptor model. *Biochim. Biophys. Acta.* **467**, 208–219 (1977)
8. Al-Sabagh, A.M.; Nasser, N.M.; Farag, A.A.; Migahed, M.A.; Eissa, A.M.F.; Mahmoud, T.: Structure effect of some amine derivatives on corrosion inhibition efficiency for carbon steel in acidic media using electrochemical and quantum theory methods. *Egypt. J. Pet.* **22**, 101–116 (2013)
9. Abd El Haleem, S.M.; Abd El-Wanees, S.; Abd El Aal, E.E.; Farouk, A.: Factors affecting the corrosion behaviour of aluminium in acid solutions. I. Nitrogen and/or sulphur-containing organic compounds as corrosion inhibitors for Al in HCl solutions. *Corros. Sci.* **68**, 1–13 (2013)
10. Doner, A.; Şahin, E.A.; Kardaş, G.; Serindağ, O.: Investigation of corrosion inhibition effect of 3-[(2-hydroxy-benzylidene)-amino]-2-thioxo-thiazolidin-4-one on corrosion of mild steel in the acidic medium. *Corros. Sci.* **66**, 278–284 (2013)
11. Daoud, D.; Douadi, T.; Issaadi, S.; Chafaa, S.: Adsorption and corrosion inhibition of new synthesized thiophene Schiff base on mild steel X52 in HCl and H<sub>2</sub>SO<sub>4</sub> solutions. *Corros. Sci.* **79**, 50–58 (2014)
12. Rbaa, M.; Lakhrissi, B.: Novel oxazole and imidazole based on 8-hydroxyquinoline as a corrosion Inhibition of mild steel in HCl solution: insights from experimental and computational studies. *Surf. Interfaces* **15**, 43–59 (2019)
13. Fergachi, O.; Benhiba, F.; Rbaa, M.; Ouakki, M.; Galai, M.; Touir, R.; Touhami, M.E.: Corrosion inhibition of ordinary steel in 5.0 M HCl medium by benzimidazole derivatives: electrochemical, UV-visible spectrometry, and DFT calculations. *J. Bio Tribo Corros.* **5**, 2–13 (2019)
14. Rbaa, M.; Benhiba, F.; Abousalem, A.S.; Galai, M.; Rouifi, Z.; Oudda, H.; Zarrouk, A.: Sample synthesis, characterization, experimental and theoretical study of the inhibitory power of new 8-hydroxyquinoline derivatives for mild steel in 1.0 M HCl. *J. Mol. Struct.* **1213**, 128155 (2020)
15. Rbaa, M.; Galai, M.; Abousalem, A.S.; Lakhrissi, B.; Touhami, M.E.; Warad, I.; Zarrouk, A.: Synthetic, spectroscopic characterization, empirical and theoretical investigations on the corrosion inhibition characteristics of mild steel in molar hydrochloric acid by three novel 8-hydroxyquinoline derivatives. *Ionics (Kiel)* **26**, 1–20 (2019)
16. Rbaa, M.; Errahmany, N.; Alaoui, K.; El Kacimi, Y.; Zarrouk, A.; Lakhrissi, B.: Electrochemical and theoretical evaluation of some quinoline derivatives as corrosion inhibitors of mild steel in acidic medium. *Anal. Bioanal. Electrochem.* **11**, 969–984 (2019)
17. Rbaa, M.; Bazdi, O.; Hichar, A.; Lakhrissi, Y.; Ounine, K.; Lakhrissi, B.: Synthesis, characterization and biological activity of new pyran derivatives of 8-hydroxyquinoline. *Eur. J. Anal. Chem.* **13**, 19–30 (2018)
18. Rbaa, M.; Lgaz, H.; El Kacimi, Y.; Lakhrissi, B.; Bentiss, F.; Zarrouk, A.: Synthesis, characterization and corrosion inhibition studies of novel 8-hydroxyquinoline derivatives on the acidic corrosion of mild steel: experimental and computational studies. *Mater. Discov.* **12**, 43–54 (2018)
19. Rouifi, Z.; Rbaa, M.; Abousalem, A.S.; Benhiba, F.; Laabaissi, T.; Oudda, H.; Zarrouk, A.: Synthesis, characterization and corrosion inhibition potential of newly benzimidazole derivatives: combining theoretical and experimental study. *Surf. Interfaces* **13**, 100442 (2020)
20. Rbaa, M.; Galai, M.; Abousalem, A.S.; Lakhrissi, B.; Touhami, M.E.; Warad, I.; Zarrouk, A.: Synthetic, spectroscopic characterization, empirical and theoretical investigations on the corrosion inhibition characteristics of mild steel in molar hydrochloric acid by three novel 8-hydroxyquinoline derivatives. *Ionics (Kiel)* **13**, 1–20 (2020)
21. Rbaa, M.; Benhiba, F.; Obot, I.B.; Oudda, H.; Warad, I.; Lakhrissi, B.; Zarrouk, A.: Two new 8-hydroxyquinoline derivatives as an efficient corrosion inhibitors for mild steel in hydrochloric acid: synthesis, electrochemical, surface morphological, UV-visible and theoretical studies. *J. Mol. Liq.* **276**, 120–133 (2018)
22. Rbaa, M.; Galai, M.; Benhiba, F.; Obot, I.B.; Oudda, H.; Touhami, M.E.; Zarrouk, A.: Synthesis and investigation of quinazoline derivatives based on 8-hydroxyquinoline as corrosion inhibitors for mild steel in acidic environment: experimental and theoretical studies. *Ionics (Kiel)* **2**, 1–19 (2018)
23. Özden, S.; Karataş, H.; Yıldız, S.; Göker, H.: Synthesis and potent antimicrobial activity of some novel 4-(5,6-dichloro-1H-benzimidazol-2-yl)-N-substituted benzamides. *Arch. Pharm. (Weinheim)* **337**, 556–562 (2004)
24. Zarrouk, A.; Hammouti, B.; Dafali, A.; Bouachrine, M.; Zarrok, H.; Boukhris, S.; Al-Deyab, S.S.: A theoretical study on the inhibition efficiencies of some quinoxalines as corrosion inhibitors of copper in nitric acid. *J. Saudi Chem. Soc.* **18**, 450–455 (2014)
25. Kannan, P.; Varghese, A.; Palanisam, K.; Abousalem, A.S.: Evaluating prolonged corrosion inhibition performance of benzyldiethylammoniumtetrachloroaluminate ionic liquid using electrochemical analysis and Monte Carlo simulation. *J. Mol. Liq.* **297**, 111855 (2020)
26. Dagdag, O.; Safi, Z.; Wazzan, N.; Erramli, H.; Guo, L.; Mkdadh, A.M.; El Harfi, A.: Highly functionalized epoxy macromolecule as an anti-corrosive material for carbon steel: computational (DFT, MDS), surface (SEM-EDS) and electrochemical (OCP, PDP, EIS) studies. *J. Mol. Liq.* **302**, 112535 (2020)
27. Kannan, P.; Karthikeyan, J.; Murugan, P.; Rao, T.S.; Rajendran, N.: Corrosion inhibition effect of novel methyl benzimidazolium ionic liquid for carbon steel in HCl medium. *J. Mol. Liq.* **221**, 368–380 (2016)
28. Palanisamy, K.; Kannan, P.; Sekar, A.: Evaluation of chromotrope FB dye as corrosion inhibitor using electrochemical and theoretical studies for acid cleaning process of petroleum pipeline. *Surf. Interfaces* **12**, 50–60 (2018)
29. Bai, L.; Feng, L.J.; Wang, H.Y.; Lu, Y.B.; Lei, X.W.; Bai, F.L.: Comparison of the synergistic effect of counterions on the inhibition of mild steel corrosion in acid solution: electrochemical, gravimetric and thermodynamic studies. *RSC Adv.* **5**, 4716–4726 (2015)
30. He, X.; Jiang, Y.; Li, C.; Wang, W.; Hou, B.; Wu, L.: Inhibition properties and adsorption behavior of imidazole and 2-phenyl-2-imidazole on AA5052 in 1.0 M HCl solution. *Corros. Sci.* **83**, 124–136 (2014)
31. Kumar, S.H.; Karthikeyan, S.: Torsemide and furosemide as green inhibitors for the corrosion of mild steel in hydrochloric acid medium. *Ind. Eng. Chem. Res.* **52**, 7457–7469 (2013)



32. Solmaz, R.: Investigation of the inhibition effect of 5-((E)-4-phenylbuta-1,3-dienylideneamino)-1,3,4-thiadiazole-2-thiol Schiff base on mild steel corrosion in hydrochloric acid. *Corros. Sci.* **52**, 3321–3330 (2010)
33. Ashassi-Sorkhabi, H.; Ghalebsaz-Jeddi, N.; Hashemzadeh, F.; Jahani, H.: Corrosion inhibition of carbon steel in hydrochloric acid by some polyethylene glycols. *Electrochim. Acta* **50**, 3848–3854 (2006)
34. Zheng, X.; Zhang, S.; Li, W.; Yin, L.; He, J.; Wu, J.: Investigation of 1-butyl-3-methyl-1H-benzimidazolium iodide as inhibitor for mild steel in sulfuric acid solution. *Corros. Sci.* **80**, 383–392 (2014)
35. Lopez, D.A.; Simison, S.N.; De Sanchez, S.R.: The influence of steel microstructure on CO<sub>2</sub> corrosion. EIS studies on the inhibition efficiency of benzimidazole. *Electrochim. Acta* **48**, 845–854 (2003)
36. Rbaa, M.; Dohare, P.; Berisha, A.; Dagdag, O.; Lakhrissi, L.; Galai, M.; Zarrouk, A.: New epoxy sugar based glucose derivatives as eco friendly corrosion inhibitors for the carbon steel in 1.0 M HCl: experimental and theoretical investigations. *J. Alloys Compd.* **833**, 154949 (2020)
37. Popova, A.; Christov, M.; Vasilev, A.: Inhibitive properties of quaternary ammonium bromides of N-containing heterocycles on acid mild steel corrosion. Part II: EIS results. *Corros. Sci.* **49**, 3290–3302 (2007)
38. Lgaz, H.; Chung, I.M.; Salghi, R.; Ali, I.H.; Chaouiki, A.; El Aoufir, Y.; Khan, M.I.: On the understanding of the adsorption of fenugreek gum on mild steel in an acidic medium: insights from experimental and computational studies. *Appl. Surf. Sci.* **463**, 647–658 (2018)
39. Growcock, F.B.; Jasinski, R.J.: Time-resolved impedance spectroscopy of mild steel in concentrated hydrochloric acid. *J. Electrochem. Soc.* **136**, 2310–2314 (1989)
40. Popova, A.; Christov, M.: Evaluation of impedance measurements on mild steel corrosion in acid media in the presence of heterocyclic compounds. *Corros. Sci.* **48**, 3208–3221 (2006)
41. El Faydy, M.; Touir, R.; Ebn Touhami, M.; Zarrouk, A.; Jama, C.; Lakhrissi, B.; Olasunkanmi, L.O.; Ebenso, E.E.; Bentiss, F.: Corrosion inhibition performance of newly synthesized 5-alkoxymethyl-8-hydroxyquinoline derivatives for carbon steel in 1 M HCl solution: experimental, DFT and Monte Carlo simulation studies. *Phys. Chem. Chem. Phys.* **20**, 20167–20187 (2018)
42. El Hezzat, M.; Assouag, M.; Zarrok, H.; Benzekri, Z.; El Assyry, A.; Boukhris, S.; Souizi, A.; Galai, M.; Touir, R.; Ebn Touhami, M.; Oudda, H.; Zarrouk, A.: Correlated DFT and electrochemical study on inhibition behavior of ethyl 6-amino-5-cyano-2-methyl-4-(p-tolyl)-4H-pyran-3-carboxylate for the corrosion of mild steel in HCl. *Der Pharma Chem.* **7**, 77–88 (2015)
43. Rbaa, M.; Abousalem, A.S.; Rouifi, Z.; Benkaddour, R.; Dohare, P.; Lakhrissi, M.; Zarrouk, A.: Synthesis, antibacterial study and corrosion inhibition potential of newly synthesis oxathiolan and triazole derivatives of 8-hydroxyquinoline: experimental and theoretical approach. *Surf. Interfaces* **19**, 100468 (2020)
44. Fouda, S.A.; Ismail, M.A.; Temraz, A.M.; Abousalem, A.S.: Comprehensive investigations on the action of cationic terthiophene and bithiophene as corrosion inhibitors: experimental and theoretical studies. *New J. Chem.* **43**, 768–789 (2019)
45. Zarrok, H.; Al-Deyab, S.S.; Zarrouk, A.; Salghi, R.; Hammouti, B.; Oudda, H.; Bouachrine, M.; Bentiss, F.: Thermodynamic characterisation and density functional theory investigation of 1,1',5,5'-tetramethyl-1H, 1'H-3,3'-bipyrazole as corrosion inhibitor of C38 steel corrosion in HCl. *Int. J. Electrochem. Sci.* **7**, 4047–4063 (2012)
46. El-Lateef, H.M.A.: Corrosion inhibition characteristics of a novel salicylidene isatin hydrazine sodium sulfonate on carbon steel in HCl and a synergistic nickel ions additive: a combined experimental and theoretical perspective. *Appl. Surf. Sci.* **501**, 144237 (2020)
47. Gnedenkov, A.S.; Mei, D.; Lamaka, S.V.; Sinebryukhov, S.L.; Mashtalyar, D. V.; Vyaliy, I.E.; Gnedenkov, S.V.: Localized currents and pH distribution studied during corrosion of MA8 Mg alloy in the cell culture medium. *Corros. Sci.* **170**, 108689 (2020)
48. Rouifi, Z.; Rbaa, M.; Benhiba, F.; Laabaissi, T.; Oudda, H.; Lakhrissi, B.; Zarrouk, A.: Preparation and anti-corrosion activity of novel 8-hydroxyquinoline derivative for carbon steel corrosion in HCl molar: computational and experimental analyses. *J. Mol. Liq.* **307**, 112923 (2020)
49. Salhi, A.; Tighadouini, S.; El-Massaoudi, M.; Elbelghiti, M.; Bouyanzer, A.; Radi, S.; El Barkany, S.; Bentiss, F.; Zarrouk, A.: Keto-enol heterocycles as new compounds of corrosion inhibitors for carbon steel in 1 M HCl: weight loss, electrochemical and quantum chemical investigation. *J. Mol. Liq.* **248**, 340–349 (2017)
50. Gobara, M.; Baraka, A.; Akid, R.; Zorainy, M.: Corrosion protection mechanism of Ce<sup>4+</sup>/organic inhibitor for AA2024 in 35% NaCl. *RSC Adv.* **10**, 2227–2240 (2020)
51. Saeedikhani, M.; Wijesinghe, S.; Blackwood, D.J.: Moving boundary simulation and mechanistic studies of the electrochemical corrosion protection by a damaged zinc coating. *Corros. Sci.* **163**, 108296 (2020)

